Journal of Environmental Management 304 (2022) 114187

Contents lists available at ScienceDirect

Journal of Environmental Management

journal homepage: www.elsevier.com/locate/jenvman

Chlorella vulgaris meets TiO_2 NPs: Effective sorbent/photocatalytic hybrid materials for water treatment application

M. Blosi [a,*], A. Brigliadori [a,**], I. Zanoni [a], S. Ortelli [a], S. Albonetti [b], A.L. Costa [a]

[a] CNR-ISTEC, Institute of Science and Technology for Ceramics – National Research Council of Italy, Via Granarolo 64, I-48018, Faenza, RA, Italy
[b] Dipartimento di Chimica Industriale "Toso Montanari", University of Bologna, Viale Del Risorgimento 4, 40136, Bologna, Italy

ARTICLE INFO

Keywords:
New wastewater treatment technology
Heavy metals biosorption
Hybrid materials
Photocatalysts
C. vulgaris
TiO_2 NPs

ABSTRACT

A new class of bio-nano hybrid catalyst useable in downstream wastewater treatment was developed. We combined the sorption potentialities of Chlorella vulgaris microalgae with the photocatalytic properties of TiO_2 NPs in order to investigate unexplored synergistic effects that could push the algal remediation technology toward a more promising cost-effective balance. We exploited non-living C. vulgaris, which keeps the biosorption properties of the living microalgae, but greatly enhancing the overall processability.

C. vulgaris biomass was coupled with TiO_2 NPs and the nanosols were then dried by means of a spray freeze drying (SFD) process able to produce highly reactive granules. A widespread physicochemical characterization supported the preparation and the performance evaluation, so highlighting the key-role of C. vulgaris/TiO_2 interaction at the colloidal state.

Heavy metal adsorption, tested for copper ions, and photocatalytic activity, assessed for Rhodamine B (RhB) photodegradation, were evaluated as key performances. The results pointed out a positive synergistic effect for hybrid samples consistent with the enhancement of metal biosorption which ranges from 103 mg g^{-1}, for pristine C. vulgaris, to about 4000 mg g^{-1}, when the biomass was coupled with the inorganic nanophase. The photocatalytic activity was well preserved with a complete RhB conversion after 1 h and even advanced in presence of SiO_2NPs into the inorganic counterpart, so increasing the kinetic constant from 8.70 to 10.7 10^{-2} min^{-1}. The results pave the way for the integration of these sorbent/photocatalytic hybrid materials into water remediation systems in an innovative sustainable design perspective.

1. Introduction

Clean water and sanitation represent the sixth of the "17 sustainable development goals" established by the United Nations in 2015 (United Nations A/RES/70/1, 2015). According to global statistics (United Nations World Water Development, 2003) a big fraction of the used water (22% in industry, 8% domestic and 70% in agriculture) is discharged as wastewater. In this scenario the development of new effective eco-friendly water treatments represents a crucial pre-condition for a sustainable advancement (United Nations Department for Economic and Social Affairs, 2013).

To date there is no standalone process able to completely treat wastewaters from the different manufacturing sectors, addressing a large variety and amount of pollutants, such as metal ions, dyes and chemicals by-products (Banat et al., 1996; Rahman Bhuiyan et al., 2016), which requires the installation of tertiary plant to fulfil the parameters set by law.

Bioremediation has emerged as a potential technology to treat industrial effluents as tertiary purification (Fazal et al., 2018; Taştan et al., 2010; Znad et al., 2018) and detailed laboratory studies (Dellamatrice et al., 2017; Ergene et al., 2009) indicated that microalgae (dead or alive) can actively remove various heavy metals and dyes (Almomani and Bohsale, 2021; Lim et al., 2010; Zeraatkar et al., 2016). Microalgae are able to convert wastewaters, CO_2 and organic residues in marketable biomass for different uses, including biofuels, converting waste in value (Judd et al., 2017; Vieira de Mendonça et al., 2021).

Heavy metals are key environmental pollutants in regions with high anthropogenic pressure and their presence, even in traces, can cause serious problems to several organisms and humans. They are stable elements, which can be bio-accumulated once passed up the food chain

* Corresponding author.
** Corresponding author.
E-mail addresses: magda.blosi@istec.cnr.it (M. Blosi), andrea.brigliadori@istec.cnr.it (A. Brigliadori).

https://doi.org/10.1016/j.jenvman.2021.114187
Received 12 April 2021; Received in revised form 26 October 2021; Accepted 24 November 2021
Available online 5 December 2021

(Suresh Kumar et al., 2015).

Biosorption is a promising technology for heavy metals removal from aqueous solutions. Algae and microalgae serve as efficient and sustainable biosorbents due to their abundance in seawater and fresh water, cost-effectiveness, reusability and high metal sorption capacities (He and Chen, 2014). Several papers deal with inactive (dead) biomass (Al Ketife et al., 2020; Vieira de Mendonça et al., 2021), that may be even more effective than active (living) one in removal of heavy metals. The inactive biomass requires neither food nor essential elements for biological growth, and may be available as waste or by-product with a noticeable advantage of cost and processing.

The cell walls of macro/micro algae consist mainly of polysaccharides, proteins, and lipids, with functional groups that confer an overall negative charge to the surface and a high binding affinity for metal cations via counterion interactions. Basically, the heavy metals absorption by non-living microalgae involves on the cell wall electrostatic interactions, van der Waals forces, covalent bonding, redox interactions, biomineralization processes.

C. vulgaris represents a suitable candidate for water bioremediation due to its great ability to remove heavy metals, dyes and to grow rapidly in most worldwide wastewaters (Axelsson et al., 2012). Despite the microalgae outstanding potentialities (Almomani and Örmeci, 2016; Volesky, 2007), nowadays new approaches and design approaches are needed to promote their advantages over conventional methods and to push their industrial implementation (Almomani et al., 2019).

In parallel, in the last decade nanostructured TiO_2 has attracted huge attention due to its photocatalytic activity which has been exploited in several fields among which the water treatment of persistent organic pollutant (POP) by advanced oxidation processes covers a relevant role (Baldisserri et al., 2018; Lolli et al., 2019; Ortelli et al., 2014).

The possibility to combine the biosorbent properties of *C. vulgaris* with inorganic photocatalytic nanoparticles represents an unexplored challenge toward the development of new hybrid multifunctional materials. So far, data available in the literature on the coupling of nanoparticles with microalgae deal mainly with eco-toxicological studies or with algal harvesting by means of magnetic nanoparticles (Almomani, 2020; Prochazkova et al., 2013; Schwertmann and Cornell, 2000). Recently, only two studies reported preliminary promising results on the possibility of merging TiO_2 nanoparticles with algae to maximize the bioremediation effectiveness against Cr^{6+} ions (Costa et al., 2019; Wang et al., 2017).

Here, the coupling of *C. vulgaris* with TiO_2 NPs allowed us to explore a new challenging frontier in the hybrid bio-nano material design. We developed a multifunction bio-nano catalyst able to combine the heavy metal absorption with the photocatalytic action. In fact, TiO_2 can photodegrade the dyes and the organic compounds typical of the industrial effluents, contemporary the microalgae can act as heavy metal sequestrant. In this framework an unexpected and never described synergistic effect enabled to emphasize the biosorption power of *C. vulgaris* when coupled with TiO_2, opening new perspectives for the algae bioremediation field and more in general for the water treatment.

Thus, the prepared materials were tested in two directions: the biosorption of Cu^{2+} ions and the photodegradation of Rhodamine B (RhB), used as a probe molecule. Such bifunctional catalysts (photocatalytic and bio-sorbent) were synthesized and tested both in suspension and in form of powder prepared by means of a spray freeze drying technique (SFD) able to remove the solvent without affecting the thermo-labile biomass and the high surface reactivity of nanostructured granules. SiO_2 NPs, known to be a photocatalytic booster for TiO_2 (Lolli et al., 2019), were also included in the design, so ensuring the optimal biosorption/photocatalytic behavior of the tricomponent hybrid materials ($TiO_2/SiO_2/$*C. vulgaris*).

2. Materials and methods

Titanium dioxide nanopowder (Aeroxide®P25, Evonik) and silica nanosol (Ludox HS-40, Grace Davison) represent the two main components combined to build up the inorganic porous matrix.

Chlorella vulgaris microalgae (Micoperi Blue Growth, Italy) is the organic counterpart coupled with the inorganic structure. Two types of *C. vulgaris* were employed (Table 1): i) fresh biomass in suspension at a concentration of 0.18 g L^{-1} (as extracted from the bioreactor, here labelled as *CV_f*) and ii) microalgae in powder prepared by means of a lyophilization process to remove the solvent (dried powder, here labelled as *CV_d*).

2.1. Colloidal preparation

Multicomponent suspensions containing both inorganic nanoparticles (TiO_2 or TiO_2/SiO_2) and *C. vulgaris,* were firstly obtained at colloidal state by heterocoagulation and then granulated. Three parameters were investigated: i) biomass weight content, ii) typology of added microalgae (fresh suspension or lyophilized powder), iii) inorganic composition (TiO_2 or TiO_2/SiO_2). Different $TiO_2/$*C. vulgaris* mass ratios were tested in order to evaluate the TiO_2 effect on the microalgae biosorption and on the other hand, how the microalgae affected TiO_2 photoactivity (Table 1).

Samples of $TiO_2/$*C. vulgaris* based on fresh microalgae added as sol are labelled with the final *_f,* while $TiO_2/$*C. vulgaris* based on dried microalgae added in powder are labelled with the final *_d.* These samples were prepared by adding a dispersion of TiO_2 in water to the microalgae suspension (0.18 g L^{-1}). The mixed samples were then kept under gentle stirring for 24 h. Typically, 100 mL of suspension contains 3 g of TiO_2 P25 and different volumes of CV_f or CV_d according to the weight ratios listed in Table 2.

TiO_2/SiO_2 inorganic samples were prepared by mixing TiO_2 suspension (0.75% wt) and SiO_2 (silica nanosol Ludox, HS40, 2.25%wt) before microalgae addition.

$TiO_2/SiO_2/$*C. vulgaris* samples, identified with the code STC, were produced by adding silica to TiO_2. Before addition, silica suspension (Ludox HS-40) was treated by means of a cation exchange resin (Dowex 50 WX8 20–50, LennTech) to adjust the pH from 9.7 to 4. Typically, the preparation of three-component samples ($SiO_2/TiO_2/$*C. vulgaris*) implies as first step the mixing of TiO_2 and SiO_2 and then the microalgae introduction. Silica sol (2.25% wt, pH 4) was dropped into TiO_2 suspension (0.75 %wt) under stirring and then ball milled for 24 h to promote the oxides interaction. Finally, according to the established weight ratios (Table 2) the right amount of microalgae suspension (CV_f, 0.18 g L^{-1}) was introduced and kept under gentle stirring (24 h).

2.2. Spray freeze granulation process

A spray-freeze drying process was applied to obtain micrometric powders starting from nanosols by means of a lab-scale apparatus (Lab-scale Granulator LS-2, Powder Pro). The sample suspension was atomized by a peristaltic pump, blowing nitrogen gas at 0.4 bar through a 100 μm nozzle and nebulized into a stirred solution of liquid nitrogen, so enabling instantaneous freezing of each generated drop. The so-frozen drops were placed into a freeze-drying equipment (LYO GT 2, SRK System Technik) with a pressure of 0.15 mbar and a temperature of −1 °C. The sublimation process is completed within 48 h, producing a highly porous granulated powder. Granulated samples are identified with the _SF code (Table 2).

Table 1
Typologies of *Chlorella vulgaris* employed in the study.

Chlorella Vulgaris	Form	Details
CV_f	Suspension	Extracted from the bioreactor
CV_d	Powder	Lyophilized

Table 2
List of all the prepared samples (suspensions and spray freeze-dried granules): sample code and detailed weight percent (%wt) composition.

SUSPENSIONS				
Sample code	**C. vulgaris type**	**TiO_2 (%wt)**	***C. vulgaris* (%wt)**	**SiO_2 (%wt)**
TiO_2	-	100	-	-
T1S3	-	25	–	75
TC-0.01_f	*fresh*	99.99	0.01	–
TC-0.06_f	*fresh*	99.94	0.06	–
TC-0.6_f	*fresh*	99.40	0.60	–
TC-6_f	*fresh*	94.00	6.00	–
STC-0.01_f	*fresh*	25.00	0.01	74.99
STC-0.06_f	*fresh*	24.98	0.06	74.96
TC-0.01_d	*dried*	99.99	0.01	–
TC-0.06_d	*dried*	99.94	0.06	–
TC-9_d	*dried*	91.00	9.00	–
GRANULATED POWDERS *(Spray freeze dried _ SF)*				
Sample code	***C. vulgaris* type**	***TiO_2* (%wt)**	***C. vulgaris* (%wt)**	**SiO_2 (%wt)**
TiO_2_SF	-	100	-	-
T1S3_SF	-	25	–	75
TC-0.01_f_SF	*fresh*	99.99	0.01	–
TC-0.06_f_SF	*fresh*	99.94	0.06	–
STC-0.01_f_SF	*fresh*	25.00	0.01	74.99
STC-0.06_f_SF	*fresh*	24.98	0.06	74.96
TC-0.01_d_SF	*dried*	99.99	0.01	–
TC-0.06_d_SF	*dried*	99.94	0.06	–
TC-9_d_SF	*dried*	91.00	9.00	

2.3. Analytical characterization

Hydrodynamic diameter and Zeta potential of suspensions were investigated by DLS/ELS techniques (dynamic/electrophoretic light scattering, Zetasizer Nano instrument ZSP, Malvern, UK). Zeta potential was monitored along a wide pH range by means of an automatic titrating system. We evaluated Z potential/pH curves also of the granulated powders after dispersion in water. The titrations were performed by adding 0.1 M KOH and 0.1 M HCl solutions to the TiO_2/*C. vulgaris* hybrid suspensions diluted at 0.1–0.5 g L^{-1}. Smoluchowski equation was applied to convert the electrophoretic mobility to Zeta potential. After 2 min for temperature equilibration, samples underwent three measurements delayed of 120 s and Zeta potential was obtained by averaging these measurements.

The granulated catalysts were observed by scanning electronic microscopy analysis using a Field Emission Scanning Electron Microscope, FE-SEM (Carl Zeiss Sigma NTS, Germany). Elemental analysis was performed by image analysis using FE-SEM coupled to an energy dispersive X-ray micro-analyzer (EDS, mod. INCA).

The suspension of *C. vulgaris* (CV_f) was dropped on a glass and observed with a 3D digital optical microscope (Hirox RH-2000) equipped with a high intensity LED lamp (5700K) and a magnification range of 35–5000x. Particle mean diameter of CV_f and CV_d was calculated as average of at least 100 particles.

The functional groups of *C. vulgaris* and TiO_2/*C. vulgaris* samples were investigated by means of UV-VIS (Lambda 750, PerkinElmer) and ATR-FTIR (Nicolet iS5, iD7, Thermo Scientific) analyses, performed in the 250–800 nm and 1800-900 cm^{-1} ranges respectively.

Specific surface area for the granulated samples was determined by N_2 physisorption apparatus (Sorpty 1750 CE instruments) and single point BET analysis methods, in which samples were pre-treated under vacuum at 120 °C.

Total Cu^{2+} concentration in water, resulting after the biosorption, was performed by ICP-OES using a 5100 Spectrometer– vertical dual view apparatus coupled with OneNeb nebulizer (Agilent Technologies, Santa Clara, CA, USA), equipped with an autosampler (S10). Analyses were conducted using a calibration curve obtained by dilution (range: 0–10 mg L^{-1}) of Cu^{2+} standard solution for ICP-OES (Sigma Aldrich, Milan, Italy). The limit of detection (LOD) at the operative wavelength of 324.754 nm was 0.01 mg L^{-1}. The measurements precision in terms of relative standard deviation (RSD %) for the analysis was always lower than 5%.

The band gap energy values of the hybrid granules were determined using the Tauc equation (Makuła et al., 2018) derived from reflectance spectra in the 250–800 nm range, collected by the PerkinElmer Lambda 750 spectrophotometer. A $BaSO_4$ tablet was considered as blank.

2.4. Biosorption tests

All the prepared samples, both in suspension and in powder, were dispersed in water and kept in contact with a solution of $CuCl_2$ (10 mg L^{-1}) at 25 °C. The tests were performed in presence of 2.5 g L^{-1} of adsorbent samples under stirring at a constant temperature of 25 °C for 30 min and at a working pH of 4.5. To quantify the biosorption, after keeping the samples in contact with Cu^{2+}, we centrifuged 8 mL of solution at 4500 rpm for 40 min by ultrafiltering the sample with centrifugal filter units (Polyethersulfone, Amicon filter 10 KDa). This way we separated the nanocatalysts from the solution quantifying by ICP-OES the not absorbed Cu^{2+} remained into the solution.

The Cu^{2+}biosorption of samples CV_f, CV_d and TSC_0.06_f was tested against Langmuir (Eq. (4)) and Freundlich (Eq. (5)) isotherms.

$$\frac{1}{q_e} = \frac{1}{q_{max}} + \frac{1}{q_{max} b C_e} \tag{3}$$

$$ln(q_e) = \ln(K_F) + \frac{1}{n}\ln(C_e) \tag{4}$$

Where q_e is the algae biosorption capacity at the equilibrium, q_{max} is the maximum heavy metal adsorbed on a unit mass of algae, C_e the Cu^{2+} concentration at the equilibrium, b a constant of the Langmuir isotherm, K_F is the adsorption capacity of algae and, n is the adsorption intensity.

Tests were carried out on volumes of 20 mL at increasing $CuCl_2$ concentrations (1, 10, 50, 100, 500, 1000 mg L^{-1}) exposed to 10 mg of *C. vulgaris* or to 50 mg of granulated hybrid biosorbent. Cu^{2+} was quantified by ICP-OES measurements on the treated solutions.

The biosorption kinetics were followed using a pseudo-first, Eq. (5), and second-order, Eq. (6)

$$\ln(q_e - q_t) = \ln(q_e) - k_1 t \tag{5}$$

$$\frac{t}{q_t} = \frac{1}{k_2 q_e^2} + \frac{1}{q_e} t \tag{6}$$

Tests were carried out on volume of 200 mL at a concentration of 10 mg L^{-1} for $CuCl_2$ and exposed to 100 mg of *C. vulgaris* or to 500 mg of granulated hybrid biosorbent. Cu^{2+} biosorption kinetic was quantified by ICP-OES measurements on the treated solutions at increasing times (1, 5, 10, 15, 20, 30, 40, 50, 60 min).

Results of adsorption and kinetic models' application are reported into table S4- S5 (ESI).

2.5. Photocatalytic tests

Photocatalytic degradation of Rhodamine B (RhB) was conducted in a beaker at room temperature, the typical set up foresees 20 mg of photocatalyst added to 200 mL of a RhB aqueous solution (0.007 g L^{-1}). Distilled water was used as blank. In order to establish an absorption/

desorption equilibrium between catalyst and RhB, the solution was kept in the dark for about 30 min, proven to be a suitable time to ensure the equilibrium. Absorption/desorption phenomena occurring during the stirring have been verified and evaluated as negligible on the overall photocatalytic reaction. The suspension was stirred and UV irradiated with intensity of 50 W m^{-2} and an average illumination wavelength of 350 nm (Osram ULTRA-Vitalux lamp 300 W). The lamp was switched-on 30 min before the beginning of the photocatalytic test to stabilize the emission power. A blank test was performed without the catalyst to verify the absence of any photolytic phenomena on RhB and the analyses were performed using a quartz cuvette as sample-holder. The degradation reaction progress was monitored at regular times (5, 10, 15, 20, 30, 40, 50, 60 min) by withdrawing and filtering (0.22 μm) 3 mL of solution and measuring the absorbance at 554 nm with a single beam spectrophotometer (UV/Vis HachLange, DR 3900). The photocatalytic activity was quantified as the photodegradation rate constant of catalyst, k (min^{-1}). The photodegradation of RhB in presence of a catalyst can be considered as a pseudo-first order reaction and can be described by equation (1):

$$\ln(C_0)\,/\,(C) = kt \tag{1}$$

According to the Lambert-Beer law, the absorbance is proportional to RhB concentration, so ln (C_0/C) is calculated by measuring initial concentration (C_0) and absorbance (A_0) and after a certain irradiation time t (A_t). The value of k was assessed by plotting ln (C_0/C) versus time (t). The conversion, calculated at t = 60 min, indicates the ratio between the amount of reagent consumed and the amount of reagent initially present in the reaction environment and it was determined by formula (2):

$$Conversion\ (\%) = (A_0 - A_t)/A_0 \text{x } 100 \tag{2}$$

3. Results and discussion

Two different forms of *Chlorella vulgaris* were added to TiO_2 NPs: microalgae in suspension as extracted by the bioreactor and microalgae in powder after being lyophilized.

Fresh microalgae, CV_f, directly extracted from the bioreactor appeared as a suspension with clearly defined round cells and average diameter of 3.8 ± 0.1 μm (Fig. 1a). On the other hand, the FE-SEM images of the lyophilized *C. vulgaris* (CV_d) showed dehydrated and collapsed multicellular aggregates, with irregular morphology and large average size of 18 ± 6 μm (Fig. 1b). DLS analyses confirmed the same dimensions, highlighting for both samples hydrodynamic diameters aligned with the microscope images (Table 3).

Fig. 1 c shows the morphology of TiO_2 P25, characterized by primary particles in the 30–60 nm dimension range, but partially agglomerated as consistent with the typical behavior of the oxide nanopowders

Table 3
DLS/ELS results collected for the prepared suspensions.

Sample code	*C. vulgaris* (wt %)	pH	Z potential (mV)	pH IEP	Zave (nm)
TiO_2	*0*	5.6	+29 ± 1	6.7	480 ± 40
CV_f	*100*	6.1	−30 ± 1	1.5	3690 ± 60
CV_d	*100*	6.5	−23 ± 1	1.8	18,000 ± 6000
TC-0.01_f	*0.01*	6.0	−27 ± 1	3.6	4500 ± 100
TC-0.06_f	*0.06*	6.0	−25 ± 1	1.8	1700 ± 200
TC-0.06_d	*0.06*	5.6	+10 ± 1	5.5	426 ± 4
STC-0.01_f	*0.01*	5.8	−37 ± 1	1.8	270 ± 1
STC-0.06_f	*0.06*	5.6	−35 ± 1	1.8	281 ± 6

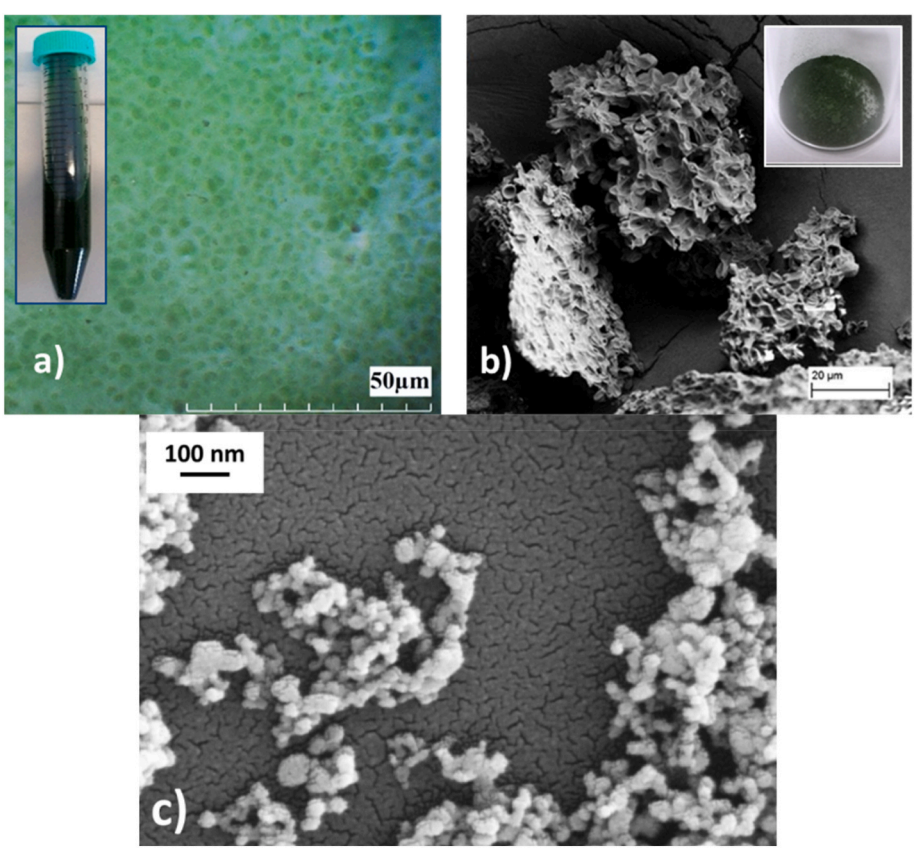

Fig. 1. a) Optical microscope image of C. *vulgaris* fresh suspension extracted from the bioreactor, sample CV_f; b) FE-SEM image collected on *C vulgaris* powder after lyophilization, sample CV_d; c) FE-SEM image collected on TiO_2 25 NPs.

prepared by high temperature processes.

3.1. Addition of TiO_2 NPs to C. vulgaris: colloidal behavior

TiO_2 P25 nanoparticles were added to microalgae suspensions by means of a colloidal process mediated by the heterocoagulation between inorganic nanoparticles and *C. vulgaris* cells.

Both FT-IR and UV-VIS spectroscopy analyses reported into Fig. S1-S2 (Electronic Supplementary Information, ESI) proved that the presence of TiO_2 did not alter the exposed functional groups of the microalgae. FT-IR spectra of *C. vulgaris* alone showed the typical microalgae spectrum, mainly composed of proteins and carbohydrates. The addition of TiO_2 NPs to produce TiO_2/*C. vulgaris* hybrid sample did not alter the absorption wavelength associated with the functional groups and only implied the intensity decreasing of the FT-IR signals as a dilution effect.

UV-VIS spectroscopy on CV_f evidenced the chlorophyll porphyrin ring absorption peaks at 680 nm e 440 nm (Mezacasa et al., 2020) (ESI, Fig S2) which were not modified in energy when combined with the inorganic phase (sample TC-0.06_f), but only presenting an increased baseline due to the scattering of solid nanoparticles and the UV absorption band typical of TiO_2.

The colloidal behavior was monitored by means of Z potential/pH titration measurements, which play a key-role in investigating the surface interaction of the two components (*C. vulgaris* and TiO_2).

As expected, TiO_2 P25 showed a positive Z potential of +28.5 mV at its natural pH (5.6) and Z potential/pH curve mainly positive along the explored pH range with an isoelectric point (IEP) placed at pH 6.7. The hydrodynamic diameter of 480 nm coarser than the observed primary particles, confirmed the presence of agglomerates, as highlighted by FE-SEM images (Fig. 1c).

Both forms of *C. vulgaris*, fresh suspension (CV_f) and lyophilized powder (CV_d), pointed out negative Z potentials placed at −30 and −23 mV respectively (Table 3) associated with very low IEP and to a negative surface charge along almost the whole explored pH range (Fig. 2a), a behavior consistent with the deprotonation of the surface functional groups (Hadjoudja et al., 2010; Hong and Brown, 2006).

The hybrid samples labelled as TC *(TiO_2/C. vulgaris)* pointed out an important difference stemming from the type of added microalgae: fresh suspension or dried powder. TC-0.06_f and TC-0.06_d samples contain the same biomass amount (0.06% wt), but they promoted two distinguished colloidal behaviors (Table 3). For sample TC-0.06_d the addition of *C. vulgaris* in powder did not affect the hydrodynamic diameter, probably due to its quick precipitation on the bottom as agglomerate. The negative surface charge of the microalgae induced a Z-potential decrease at +10 mV (Table 3), but without a surface charge inversion. Z potential/pH curve appeared as an averaged profile of the two components (microalgae and TiO_2) with an IEP at pH 5.5 close to TiO_2 alone (Fig. 2a). These results show how the presence of *C. vulgaris*, as lyophilized powder (CV_d), has a negligible influence on the colloidal behavior of TiO_2, assuming a very weak interaction (or absence of interaction) between the algal phase and the inorganic one.

On the contrary, *C. vulgaris* fresh suspension added into sample TC-0.06_f modified the colloidal characteristics of TiO_2 despite the low amount of microalgae, confirming the presence of a strong surface interaction between *C. vulgaris* and TiO_2. For TC-0.06_f the influence of the microalgae was noticeable both in terms of hydrodynamic diameter, assessed around 1.7 μm, a value closer to the biomass cells and in terms of Z-potential, which highlighted an abrupt surface charge switching (Table 3) to −25 mV. Furthermore, Z potential/pH curve overlapped the curve of fresh microalgae alone, showing an abrupt migration toward the negative zone associated with a marked shift of IEP to low values (Fig. 2b).

These data are consistent with a TiO_2/microalgae self-assembling phenomenon driven by the surface electrostatic interaction and defined for colloids as heterocoagulation (Lolli et al., 2019). *C. vulgaris* surrounds TiO_2 NPs surface, embedding the inorganic phase with a sponge-like effect, so exposing its functional groups to the environment. This behavior was detected for all the samples prepared with fresh *C. vulgaris* in suspension and never observed adding the biomass in powder (CV-d), which probably is too aggregated and low reactive to promote an effective surface interaction with TiO_2.

We also measured Z potential/pH curves of samples at increasing concentration of microalgae, as reported in Fig. S3 (ESI). The data confirmed once again the different interaction occurring if we add fresh or lyophilized microalgae to TiO_2. The addition of fresh biomass strongly affected Z potential/pH curves even at very low biomass content (0.01% wt), confirming the noticeable interaction of fresh *C. vulgaris* with the inorganic nanoparticles. In fact, we detected a significant IEP shifting from 6.5 to 3.6 at the lowest algae content in sample TC-0.01_f. Probably at such low biomass concentration only a partial covering of the inorganic phase occurred, because at acid pH the curve did not completely overlap the biomass profile. As aforementioned, the situation was different for sample TC-0.06_f, where the complete overlapping with the algal curve alone and the displacement of the isoelectric point at pH < 2 were consistent with a complete surface saturation. The same behavior was observed for an increased algal concentration at 6% wt (TC-6_f), confirming that probably the maximum surface coverage of TiO_2 was already achieved for a biomass percentage of 0.06% wt.

On the contrary, in presence of dried *C. vulgaris* (ESI, Fig. S3b), not

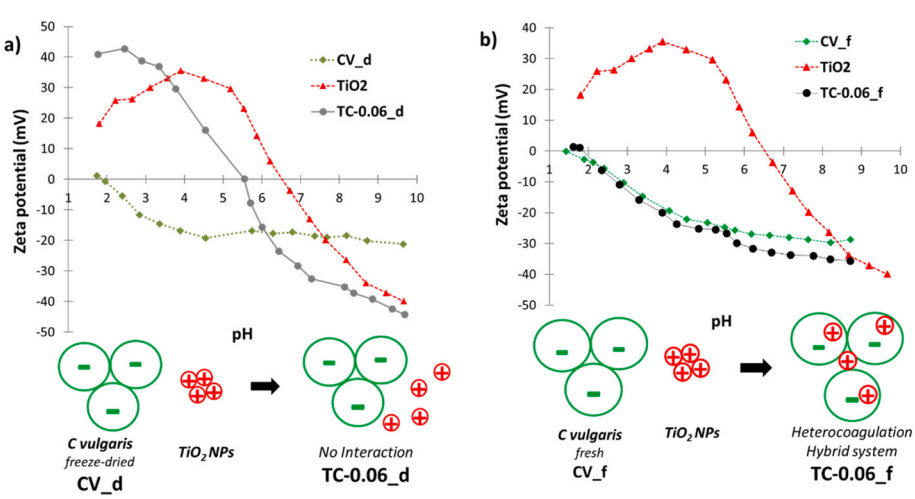

Fig. 2. Z potential/pH titration curves of samples: a) TC-0.06_d (●) compared with TiO_2 (▲) and CV_d (◆); b) TC-0.06_f (●), compared with TiO_2 (▲) and CV_f (◆).

able to interact with the inorganic NPs, Z-potential titration curves appeared simply as the averaged profiles of the two components in suspension, excluding again the establishment of marked interaction between the involved components. By increasing the biomass content until a value of 9% wt (TC-9_d) the curve moved toward the negative zone closer to the biomass one, but with the IEP still around pH 4, which only suggested an averaged profile among the components in suspension due to the very high algal concentration.

3.2. Three components suspensions: $SiO_2/TiO_2/C.$ vulgaris

Samples involving three components: TiO_2, SiO_2 and *C. vulgaris*, are labelled with the STC code and were prepared in order to enhance the photocatalytic activity of TiO_2, because silica nanoparticles are known to be a photocatalytic booster for titania nanoparticles (Lolli et al., 2019). Silica was added in excess with respect to TiO_2 as detailed in Table 2 and according to our previous study aimed to improve the photocatalytic activity (Lolli et al., 2019). Since the best surface interaction with TiO_2 was detected by adding fresh biomass, three components samples were prepared in presence of fresh biomass only (CV_f).

Fig. S4 (ESI) shows the Z-potential/pH curves collected for the $SiO_2/TiO_2/C.$ *vulgaris* three components samples (STC-0.01_f, STC-0.06_f). The presence of silica did not alter the Z potential/pH curve of TC_f samples alone, because of its strong acidic behavior and IEP naturally set at pH < 2. shifted toward slightly negative values, but improved the particle dispersion, as highlighted by the smaller hydrodynamic diameter reported in Table 3.

3.3. Characterization of the spray-freeze dried hybrid samples

All the prepared samples were spray freeze dried providing easy to handle granulated powders, more suitable than suspensions to be implemented in water treatment plants. Once spray frozen, the dried solid still reflected the differences between fresh microalgae (CV_f) or dried one (CV_d) (Fig. 3). In fact, for the same algal content, samples synthesized with fresh biomass appeared in form of homogeneous green colored powder (TC-0.06_f_SF) supporting the presence of a biomass/TiO_2 interaction and of an optimal dispersion in the colloidal form. On the other hand, sample TC-0.06_d_SF, added with the lyophilized biomass, appeared as a white powder with green spots, due to the not optimal interaction verified in suspension.

FE-SEM analyses of the spray-freeze dried samples revealed micrometric spherical granules characterized by a surface porous nanostructure (Fig. 4 a-b), suitable to be handled and applied as powder sorbent medium.

The presence of silica promoted the compactness of the granules, as confirmed by our previous studies (Lolli et al., 2019), while *C. vulgaris* did not affect their morphology and resistance. The granules size ranged from 1 to about 100 μm, with the most frequent dimension at 20–30 μm. As expected, the inorganic phase provided the skeleton to the hybrid structure, and the microalgae was surrounded by the inorganic network . Nevertheless, it was possible to distinguish *C. vulgaris* only in few images, showing the typical microalgae cells intimately linked to the inorganic phase (Fig. 4c) as consistent with the EDX mapping analysis reported in Fig. S5 (ESI).

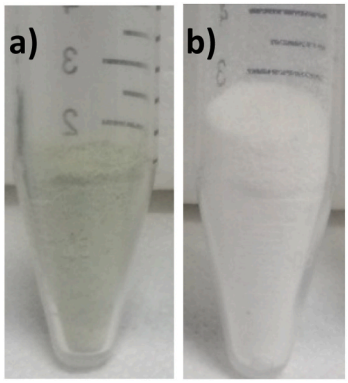

Fig. 3. Spray-freeze dried samples containing the same microalgae amount: a) TC-0.06_f_SF prepared with fresh *C. vulgaris*; b) TC-0.06_d_SF prepared with lyophilized *C. vulgaris*.

Specific surface area was measured on samples after spray freeze granulation (Table 4). TiO_2 granules exhibited a value of 63 $m^2\ g^{-1}$ aligned with the material before granulation and with the literature reported for TiO_2 P25 (Li et al., 2020). Instead, SiO_2 granules, coming from a well dispersed nanosilica suspension showed a very high surface area (203 $m^2\ g^{-1}$). The coupling of TiO_2 with SiO_2, the latter acting as particle dispersant, increased the surface area of the combined TiO_2/SiO_2 sample until the value of 223 $m^2\ g^{-1}$. On the contrary, the microalgae pointed out a low SSA (2 $m^2\ g^{-1}$), as typical of the organic matrices and when combined to TiO_2 in form of fresh suspension promoted an overall SSA reduction. For sample TC-0.01_f_SF, involving a very low *C. vulgaris* content (0.01% wt), the biomass effect was negligible with a final measured SSA of 63 $m^2\ g^{-1}$, the same one measured for TiO_2 alone. As the biomass content was increased at 0.06% wt (TC-0.06_f_SF) the value dropped at 39 $m^2\ g^{-1}$, keeping in this range (37 $m^2\ g^{-1}$) even for a high biomass content of 6%wt (TC-6_f_SF). The situation turned different for the three components granules, $SiO_2/TiO_2/C.$ *vulgaris,* where the SSA was mainly driven by the presence of silica, which markedly increased values to higher range and appeared scarcely affected by the presence of biomass. Specific surface area of 229 $m^2\ g^{-1}$ was ascribed to sample STC-0.01_f_SF containing the lowest biomass percentage (0.01% wt) and a value of 169 $m^2\ g^{-1}$ was measured for sample STC-0.06_f_SF, with a biomass content of 0.06% wt. The granules coming from suspensions prepared with lyophilized powder of *C. vulgaris* showed for all algal concentrations (0.06% and 9% wt) the surface area value typical of TiO_2 (about 70 $m^2\ g^{-1}$), further demonstrating the lack of interaction between the parties at the colloidal state.

3.4. Biosorption activity of the hybrid granules

Prepared hybrid samples were tested for heavy metals absorption in presence of 10 mg mL^{-1} of $CuCl_2$, selected as probe metal at a concentration aligned with the value reported in the literature dealing with heavy metal biosorption by microalgae (Goher et al., 2016; Mehta and Gaur, 2001; Saavedra et al., 2018; Varma and Misra, 2018; Zeraatkar et al., 2016). The biosorption of heavy metals from wastewater by means of solid sorbents is typically affected by several factors such as temperature, pH, sorbent dose and contact time (Srivastava et al., 2015). Despite high pH enhances the activity of *C. vulgaris* functional groups, we selected pH 4.5 in order to prevent precipitation of $Cu(OH)_2$ occurring at pH 6 and coagulation of *C. vulgaris* expected at the isoelectric point (IEP pH 2) (Mallick, 2003; Procházková et al., 2012). Table 5 lists the absorption data assessed for the single components used to prepare the hybrid granules (CV_f, CV_d, TiO_2, SiO_2, T1S3_SF). The results confirmed that only *C. vulgaris* has a sorption capability for Cu^{2+} ions. CV_f showed a biosorption of 103 mg g^{-1} consistent with the literature (Suresh Kumar et al., 2015; Zeraatkar et al., 2016), as expected the dried biomass (CV_d) was less active with a biosorption of 15 mg g^{-1} and the inorganic components, TiO_2 and SiO_2, evidenced negligible values of 0.3 mg g^{-1}.

The ions absorption measured for all the samples in suspension before granulation were reported into the Electronic Supplementary Information. Here the discussion is focused on the granulated samples, which ensured the same functional performances of suspensions, but having the enormous technological advantage of being easier to handle and potentially more applicable to large scale plant.

Biosorption data evidenced a synergistic effect verified only for samples prepared with fresh algal suspension and probably promoted by

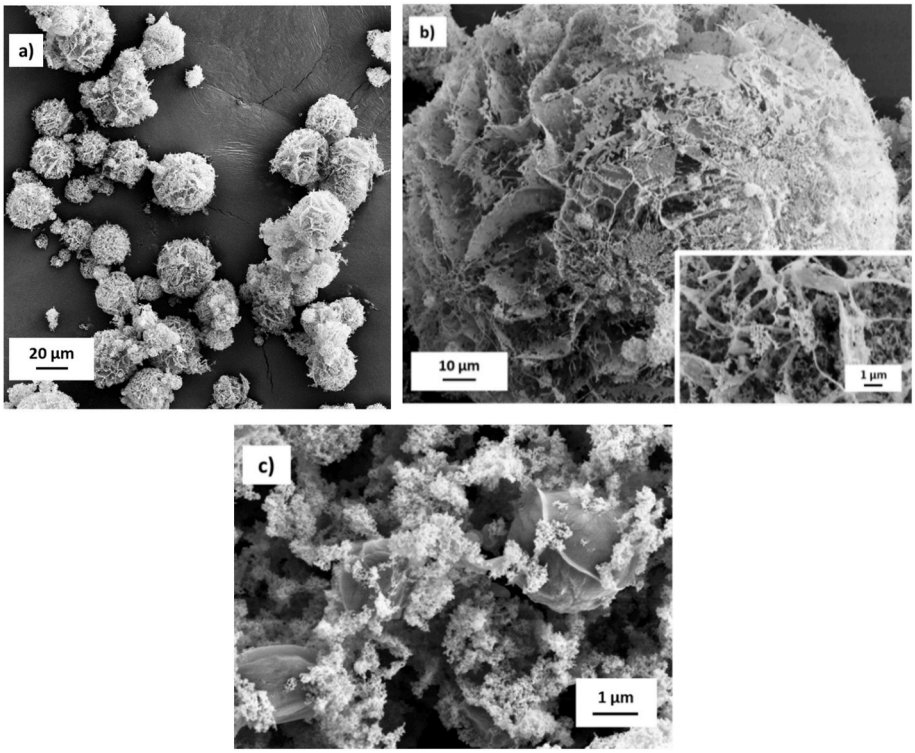

Fig. 4. FE-SEM images collected on the spray freeze dried samples: a) STC-0.01_f_SF; b) STC-0.06_f_SF, the inset at higher magnification highlights the nanostructure; c) TC-0.06_f_SF, detail of *C. vulgaris* cells embedded into the TiO_2 matrix.

Table 4
Specific surface area (SSA) measured by BET method for spray freeze dried samples.

Sample code	Components	SSA ($m^2\ g^{-1}$)
CV_d	*C. vulgaris*	2
TiO_2_SF	*TiO_2*	63
SiO_2_SF	*SiO_2*	203
T1S3_SF	*TiO_2/SiO_2*	223
TC-0.01_f_ SF	*TiO_2/C. vulgaris*	63
TC-0.06_f_SF	*TiO_2/C. vulgaris*	39
TC-0.6_f_ SF	*TiO_2/C. vulgaris*	37
STC-0.01_f_SF	*SiO_2/TiO_2/C. vulgaris*	229
STC-0.06_f_SF	*SiO_2/TiO_2/C. vulgaris*	169
TC-0.06_d_SF	*TiO_2/C. vulgaris*	67
TC-9_d_SF	*TiO_2/C. vulgaris*	70

Table 5
Cu^{2+}absorption measured for the single components of the hybrid materials.

Sample code	Absorption($mg_{Cu^{2+}}/g_{sample}$)
CV_f	103
CV_d	15.3
TiO_2_SF	0.33
SiO_2_SF	0.32
T1S3_SF	0.43

C. vulgaris/TiO_2 surface interactions, as verified by the Z potential profiles. For the hybrid granules containing fresh *C. vulgaris,* in fact, we observed metal absorption data extremely higher than the values expected by the weighted average based on composition and improved by increasing the algal content (Fig. 5a). While for samples added with the dried biomass we measured absorption of Cu^{2+} consistent with the expected theoretical value (Fig. 5b).

For example, TC-0.06_f_SF containing fresh *C. vulgaris* absorbed 3.00

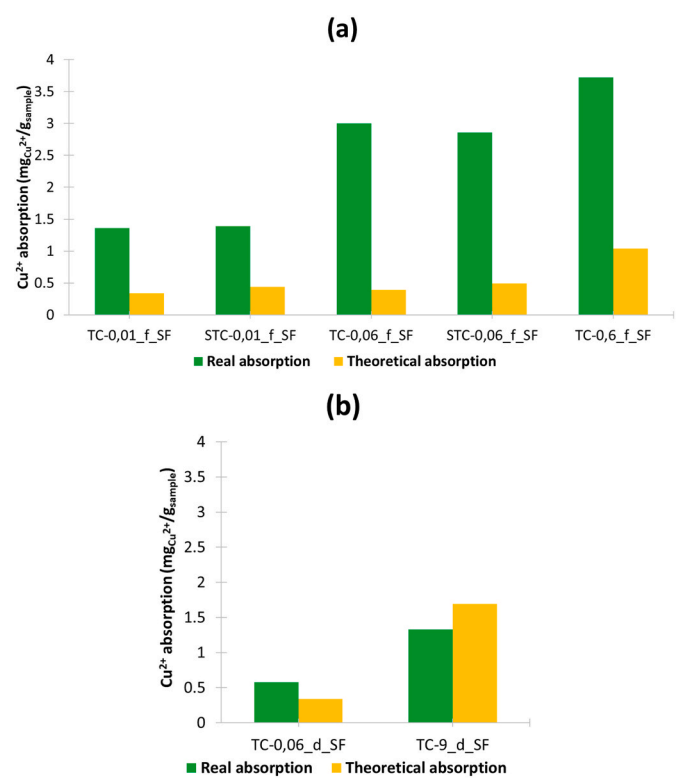

Fig. 5. Cu^{2+}absorption measured for the hybrid granules and compared with the expected theoretical absorption: a) samples prepared with fresh *C. vulgaris*; b) samples prepared with dried *C. vulgaris*.

mg of Cu^{2+} for gram of granule, while TC-0.06_d_SF, prepared by adding the same amount of *C. vulgaris* in powder, absorbed 0.58 mg g^{-1}, value close to the theoretical absorption calculated as weighted average on composition (7) (Table 6).

$$\textbf{Theortical Absorption}\ (TC-0.06\_d\_SF) = (TiO_2\_SF)_{abs} \times (TiO_2\%wt) + (CV\_d)_{abs} \times (C.\ vulgaris\ \%wt) = 0.33. \times (99.94/100) + 15.3 \times (0.06/100) = \mathbf{0.34} \quad (7)$$

The outstanding performance measured for the samples containing fresh biomass was further highlighted by calculating the biosorption value per gram of biomass contained into the hybrid granule (Table 6, Fig. 6). Such data evidenced the significant improvement in biosorption capability occurring when *C. vulgaris* is coupled and bonded with TiO_2, behavior never reported in the literature so far. We hypothesized that in case of TiO_2/*C. vulgaris* interaction, the inorganic phase acts supporting and dispersing efficiently the microalgae and maximizes the cell wall exposure bearing the functional groups responsible for the heavy metal sorption. This way the biosorption efficiency resulted to be boosted of an order of magnitude (4460 mg g^{-1}) with respect to CV_f, the fresh algal suspension alone (103 mg g^{-1}). As pointed out by collected data, such synergistic effect was verified for the material in suspension (ESI), and it was kept after the spray-freeze drying treatment on granules as well (Table 6). Based on the biosorption value per gram of *C. vulgaris* we noticed that the biomass specific efficiency was maximized for the lowest algal contents, condition that probably makes the algal dispersion onto TiO_2 surface more efficient.

However, samples containing a biomass concentration of 0.06% wt (TC-0.06_f_SF and STC-0.06_f_SF) represent the best compromise to maximize the synergistic effect and ensure a good absorption efficiency both on the biomass and the hybrid granules.

Samples prepared by adding dried *C. vulgaris* (CV_d), not able to interact at colloidal stage with TiO_2 NPs, did not involve any synergistic outcome either in suspension (ESI) or after the spray granulation treatment, with algal biosorption values (14.6 and 11.4 mg g^{-1}) very close to the performance of the dried biomass alone (15.3 mg g^{-1}).

As pointed out by Table 6 and Fig. 6 the presence of SiO_2 did not alter the biosorption capability of *C. vulgaris* ensuring an optimal absorption performance for the three components samples as well.

3.5. Photocatalytic activity of the hybrid granules

The chance of coupling a photocatalytic phase with a sorbent one emphasizes the environmental application potentialities of the here presented technology. The photocatalytic activity was investigated by means of photodegradation tests of a probe organic dye (Rhodamine B, RhB) under UV irradiation for 60 min.

Electronic Supplementary Information reports the photocatalytic results measured for the colloidal samples, here we discuss the performances measured on the spray freeze dried granules. As described in our previous study (Ortelli et al., 2014), the white color of RhB obtained after irradiation and the not shifted band at 554 nm are consistent with the complete chromophore degradation of RhB.

TiO_2 P25 is a well-known photocatalyst and its activity was here confirmed by an assessed kinetic constant of $10.4 \cdot 10^{-2}$ min^{-1} in suspension (ESI) and of $8.7 \cdot 10^{-2}$ min^{-1} after granulation (TiO_2_SF), with an almost total conversion achieved within 60 min of irradiation (99%)

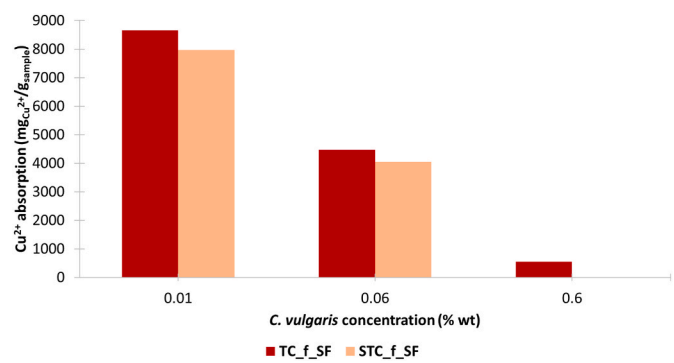

Fig. 6. Absorption of Cu^{2+} ions per gram of *C. vulgaris* for samples prepared with fresh biomass.

Table 7
Photocatalytic data collected on the prepared hybrid materials after spray freeze drying. Kinetic constants are calculated on 30 min of reaction.

Sample code	Components	k x 10^{-2} (min^{-1})	Conversion 60 min (%)
TiO_2_SF	TiO_2	8.70	99
T1S3_SF	SiO_2/TiO_2	9.45	100
TC-0.01_f_SF	TiO_2/CV_f	5.02	98
TC-0.06_f_SF	TiO_2/CV_f	2.44	92
TC-0.6_f_SF	TiO_2/CV_f	2.50	88
STC-0.01_f_SF	SiO_2/TiO_2/CV_f	11.22	100
STC-0.06_f_SF	SiO_2/TiO_2/CV_f	10.67	100
TC-0.06_d_SF	TiO_2/CV_d	8.37	98
TC-9_d_SF	TiO_2/CV_d	4.29	97

Table 6
Cu^{2+}absorption measured for the prepared hybrid materials after granulation.

Sample code	Components	*C vulgaris* Biosorption[a] ($mg_{Cu}{}^{2+}/g_{C.\ Vulgaris}$)	Granules Absorption ($mg_{Cu}{}^{2+}/g_{sample}$)	Theoretical Absorption[b] ($mg_{Cu}{}^{2+}/g_{sample}$)
TC-0.01_f_SF	TiO_2/CV_f	8650	1.36	0.34
TC-0.06_f_SF	TiO_2/CV_f	4460	3.00	0.39
TC-0.6_f_SF	TiO_2/CV_f	553	3.72	1.04
STC-0.01_f_SF	SiO_2/TiO_2/CV_f	7960	1.39	0.44
STC-0.06_f_SF	SiO_2/TiO_2/CV_f	4050	2.86	0.49
TC-0.06_d_SF	TiO_2/CV_d	14.6	0.58	0.34
TC-9_d_SF	TiO_2/CV_d	11.4	1.33	1.69

[a] *Absorption value normalized on C. vulgaris content after subtracting the inorganic phase contribution.*
[b] *Theoretical absorption calculated as weighted average on composition.*

and by following a first order kinetic profile. On the other hand, both *C. vulgaris* types, fresh and dried, did not show photocatalytic activity, without any photodegradation phenomenon during the irradiation time.

Samples with increasing content of biomass were tested and once again the results pointed out the differences occurring between the addition of fresh or dried microalgae during the preparation.

Increasing contents of fresh *C. vulgaris* (CV_f) affected the dye degradation rate with detrimental outcomes on the photocatalytic performance, which was not prevented, but delayed, as proven by the reduction of kinetic constants and of conversion percentage (Table 7). The irradiation time of 60 min allowed achieving almost complete conversion for all the samples excepting for TC-0.6_f_SF because of the high fresh biomass content. *C. vulgaris* at the interface seems not to suppress the activity, quenching the radicals or modifying the band gap energy (ESI), but most likely it acts by screening TiO_2 surface, reducing the exposed area to UV radiation and delaying the photodegradation reaction.

In contrast, the photocatalytic performance of samples prepared by adding lyophilized *C. vulgaris* was only slightly affected by the microalgae both as granule form (Table 7) and in suspension (ESI), with k values really depleted only for very high biomass concentration, as a further indirect evidence of the poor surface interaction occurring in this set of samples between TiO_2 and *C. vulgaris*.

Nevertheless, we figured out that among the prepared materials the most interesting for a water remediation perspective are the catalysts prepared with fresh biomass able to trigger synergistic effects in heavy metal biosorption. To overcome the photocatalytic depletion assessed in presence of fresh *C. vulgaris* we added silica which enabled the abrupt increase of the granules surface area (Table 4) and of the photocatalytic activity, as expressed by the k increasing of sample T1S3_SF. In fact, the three components samples containing silica showed kinetic constants comparable or even higher than TiO_2 (Table 7, Fig. 7) making these sorbent/photoactive hybrid catalysts actually promising for water treatment applications.

Samples STC-0.01_f_SF and STC-0.06_f_SF, prepared with silica and two different algae contents (0.01% and 0.06% wt) highlighted the best photodegradation kinetic constants with a complete conversion (100%).

Based on the overall functional properties, sample STC-0.06_f_SF was identified as the optimal combination of components useful to successfully combine and maximize photocatalytic activity and heavy metal sorption.

4. Conclusions

We presented novel sorbent/photoactive hybrid catalysts for water treatment applications, showing unexpected synergistic effects coming by coupling TiO_2 NPs with *C. vulgaris* microalgae.

We developed the catalysts by mixing in suspension TiO_2 P25 with the biomass and then achieving the hybrid porous granules by means of a spray-freeze drying process.

Surface interaction between TiO_2 and *C. vulgaris* plays a key role in promoting the functional properties. In fact, the biosorption capability of the microalgae was greatly enhanced for the hybrid samples containing fresh *C vulgaris* able to interact with TiO_2. We hypothesized that the inorganic phase supports the biomass, acting as dispersant and maximizing the algal sorption performance. On the other hand such TiO_2/biomass interaction was partially detrimental for the photocatalytic performance, implying a reduction in terms of photodegradation velocity, which was successfully overcome by adding silica NPs, able to boost the photocatalytic activity of TiO_2 without interfering with biosorption activity.

The possibility of exploiting dead biomass and the coupling of two functionalities in a synergistic system pave the way to new and exciting potentialities for microalgae in water treatment application and greatly increase the value of the proposed technology in a sustainability-driven perspective. Dead biomass can be easily manipulated and engineered, for example testing is ongoing on sample STC-0.06_f embedded into reusable biopolymeric scaffolds acting as photocatalytic/sorbents filters.

The development of microalgae with improved efficiency will address the strategic challenges of the European Green Deal, the priority action plan presented in 2019 to make the EU's economy sustainable which will guide most of the Horizon Europe work program. The sustainable character of the advanced hybrid materials can be even emphasized if we consider that microalgae represent a promising

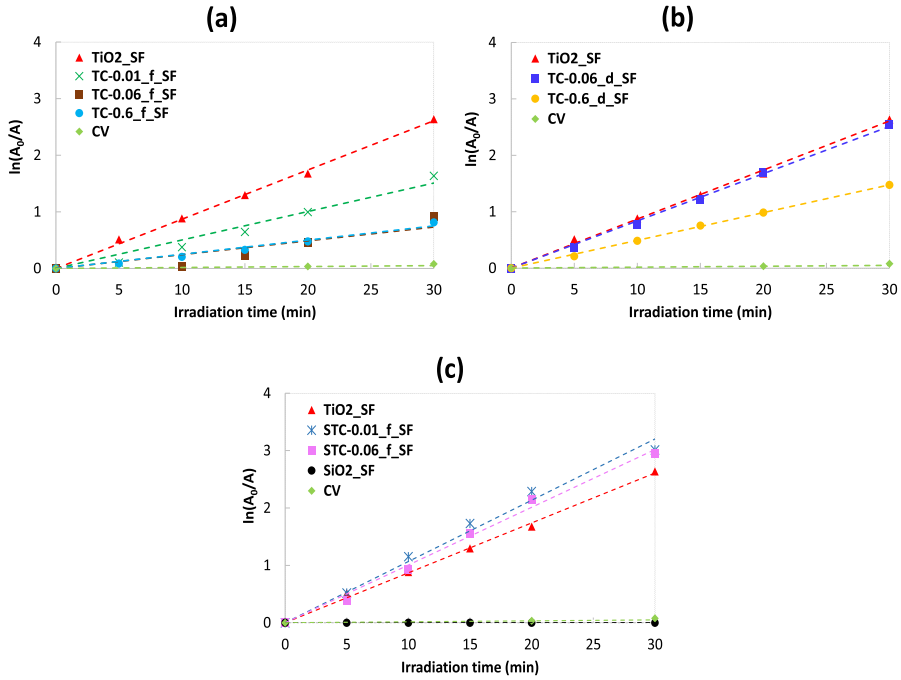

Fig. 7. Photocatalytic performances collected on RhB photodegradation for TiO_2 hybrid granules prepared with: a) fresh *C. vulgaris*; b) lyophilized *C. vulgaris*; c) SiO_2 and fresh *C. vulgaris*.

renewable energy source of the future, which can grow in wastewater sites and once exhausted and properly separated from the inorganic support could be converted into biofuel.

Credit author statement

Magda Blosi: Writing – original draft, Conceptualization, Supervision, Investigation, reviewing editing. **Andrea Brigliadori**: Writing – original draft, Investigation, Validation, Data curation, reviewing editing. **Ilaria Zanoni**: Investigation, Data curation, reviewing editing. **Simona Ortelli**: Data curation; reviewing editing. **Stefania Albonetti:** Supervision, Data curation. **Anna Luisa Costa**: funding acquisition, reviewing editing.

Declaration of competing interest

The authors declare that they have no known competing financial interests or personal relationships that could have appeared to influence the work reported in this paper.

Acknowledgements

The research leading to these results has received funding from the project "SOS-Acqua" funded by the Italian Ministry of Defence within the Military National Research Program PNRM 2019. Micoperi Blue Growth srl (Ravenna, IT) is acknowledged for providing Chlorella vulgaris microalgae.

Appendix A. Supplementary data

Supplementary data to this article can be found online at https://doi.org/10.1016/j.jenvman.2021.114187.

References

Al Ketife, A.M.D., Al Momani, F., Judd, S., 2020. A bioassimilation and bioaccumulation model for the removal of heavy metals from wastewater using algae: new strategy. Process Saf. Environ. Protect. 144, 52–64. https://doi.org/10.1016/j.psep.2020.07.018.

Almomani, F., 2020. Algal cells harvesting using cost-effective magnetic nano-particles. Sci. Total Environ. 720, 137621. https://doi.org/10.1016/j.scitotenv.2020.137621.

Almomani, F., Al Ketife, A., Judd, S., Shurair, M., Bhosale, R.R., Znad, H., Tawalbeh, M., 2019. Impact of CO 2 concentration and ambient conditions on microalgal growth and nutrient removal from wastewater by a photobioreactor. Sci. Total Environ. 662, 662–671. https://doi.org/10.1016/j.scitotenv.2019.01.144.

Almomani, F., Bohsale, R.R., 2021. Bio-sorption of toxic metals from industrial wastewater by algae strains Spirulina platensis and Chlorella vulgaris: application of isotherm, kinetic models and process optimization. Sci. Total Environ. 755, 142654. https://doi.org/10.1016/j.scitotenv.2020.142654.

Almomani, F.A., Örmeci, B., 2016. Performance of Chlorella Vulgaris, Neochloris Oleoabundans, and mixed indigenous microalgae for treatment of primary effluent, secondary effluent and centrate. Ecol. Eng. 95, 280–289. https://doi.org/10.1016/j.ecoleng.2016.06.038.

Axelsson, L., Franzén, M., Ostwald, M., Berndes, G., Lakshmi, G., Ravindranath, N.H., 2012. Perspective: jatropha cultivation in southern India: assessing farmers' experiences. Biofuel Bioprod. Biorefin. 6, 246–256. https://doi.org/10.1002/bbb.

Baldisserri, C., Ortelli, S., Blosi, M., Costa, A.L., 2018. Pilot- plant study for the photocatalytic/electrochemical degradation of Rhodamine B. J. Environ. Chem. Eng. 6, 1794–1804. https://doi.org/10.1016/j.jece.2018.02.008.

Banat, I.M., Nigam, P., Singh, D., Marchant, R., 1996. Microbial decolorization of textile-dye-containing effluents: a review. Bioresour. Technol. 58, 217–227. https://doi.org/10.1016/S0960-8524(96)00113-7.

Costa, I.G.F., Terra, N.M., Cardoso, V.L., Batista, F.R.X., Reis, M.H.M., 2019. Photoreduction of chromium(VI) in microstructured ceramic hollow fibers impregnated with titanium dioxide and coated with green algae Chlorella vulgaris. J. Hazard Mater. 379, 120837. https://doi.org/10.1016/j.jhazmat.2019.120837.

Dellamatrice, P.M., Silva-Stenico, M.E., Moraes, L.A.B. de, Fiore, M.F., Monteiro, R.T.R., 2017. Degradation of textile dyes by cyanobacteria. Braz. J. Microbiol. 48, 25–31. https://doi.org/10.1016/j.bjm.2016.09.012.

Ergene, A., Ada, K., Tan, S., Katircioğlu, H., 2009. Removal of Remazol Brilliant Blue R dye from aqueous solutions by adsorption onto immobilized Scenedesmus quadricauda: equilibrium and kinetic modeling studies. Desalination 249, 1308–1314. https://doi.org/10.1016/j.desal.2009.06.027.

Fazal, T., Mushtaq, A., Rehman, F., Ullah Khan, A., Rashid, N., Farooq, W., Rehman, M.S. U., Xu, J., 2018. Bioremediation of textile wastewater and successive biodiesel production using microalgae. Renew. Sustain. Energy Rev. 82, 3107–3126. https://doi.org/10.1016/j.rser.2017.10.029.

Goher, M.E., El-Monem, A.M.A., Abdel-Satar, A.M., Ali, M.H., Hussian, A.E.M., Napiórkowska-Krzebietke, A., 2016. Biosorption of some toxic metals from aqueous solution using non-living algal cells of Chlorella vulgaris. J. Elem. 21, 703–714. https://doi.org/10.5601/jelem.2015.20.4.1037.

Hadjoudja, S., Deluchat, V., Baudu, M., 2010. Cell surface characterisation of Microcystis aeruginosa and Chlorella vulgaris. J. Colloid Interface Sci. 342, 293–299. https://doi.org/10.1016/j.jcis.2009.10.078.

He, J., Chen, J.P., 2014. A comprehensive review on biosorption of heavy metals by algal biomass: materials, performances, chemistry, and modeling simulation tools. Bioresour. Technol. 160, 67–78. https://doi.org/10.1016/j.biortech.2014.01.068.

Hong, Y., Brown, D.G., 2006. Cell surface acid-base properties of Escherichia coli and Bacillus brevis and variation as a function of growth phase, nitrogen source and C:N ratio. Colloids Surf. B Biointerfaces 50, 112–119. https://doi.org/10.1016/j.colsurfb.2006.05.001.

Judd, S.J., Al Momani, F.A.O., Znad, H., Al Ketife, A.M.D., 2017. The cost benefit of algal technology for combined CO2 mitigation and nutrient abatement. Renew. Sustain. Energy Rev. 71, 379–387. https://doi.org/10.1016/J.RSER.2016.12.068.

Li, D., Song, H., Meng, X., Shen, T., Sun, J., Han, W., Wang, X., 2020. Effects of particle size on the structure and photocatalytic performance by alkali-treated TiO2. Nanomaterials 10, 1–14. https://doi.org/10.3390/nano10030546.

Lim, S.L., Chu, W.L., Phang, S.M., 2010. Use of Chlorella vulgaris for bioremediation of textile wastewater. Bioresour. Technol. 101, 7314–7322. https://doi.org/10.1016/j.biortech.2010.04.092.

Lolli, A., Blosi, M., Ortelli, S., Costa, A.L., Zanoni, I., Bonincontro, D., Carella, F., Albonetti, S., 2019. Innovative synthesis of nanostructured composite materials by a spray-freeze drying process: efficient catalysts and photocatalysts preparation. Catal. Today 334, 193–202. https://doi.org/10.1016/j.cattod.2018.11.022.

Makuła, P., Pacia, M., Macyk, W., 2018. How to correctly determine the band gap energy of modified semiconductor photocatalysts based on UV-vis spectra. J. Phys. Chem. Lett. 9, 6814–6817. https://doi.org/10.1021/acs.jpclett.8b02892.

Mallick, N., 2003. Biotechnological potential of Chlorella vulgaris for accumulation of Cu and Ni from single and binary metal solutions. World J. Microbiol. Biotechnol. 19, 695–701. https://doi.org/10.1023/A:1025104918352.

Mehta, S.K., Gaur, J.P., 2001. Removal of Ni and Cu from single and binary metal solutions by free and immobilized. Chlorella vulgaris 271, 261–271.

Mezacasa, A.V., Queiroz, A.M., Graciano, D.E., Pontes, M.S., Santiago, E.F., Oliveira, I.P., Lopez, A.J., Casagrande, G.A., Scherer, M.D., dos Reis, D.D., Oliveira, S.L., Caires, A. R.L., 2020. Effects of gold nanoparticles on photophysical behaviour of chlorophyll and pheophytin. J. Photochem. Photobiol. Chem. 389, 112252. https://doi.org/10.1016/j.jphotochem.2019.112252.

Ortelli, S., Blosi, M., Albonetti, S., Vaccari, A., Dondi, M., Costa, A.L., 2014. TiO2based nano-photocatalysis immobilized on cellulose substrates. J. Photochem. Photobiol. Chem. 276, 58–64. https://doi.org/10.1016/j.jphotochem.2013.11.013.

Prochazkova, G., Safarik, I., Branyik, T., 2013. Harvesting microalgae with microwave synthesized magnetic microparticles. Bioresour. Technol. 130, 472–477. https://doi.org/10.1016/J.BIORTECH.2012.12.060.

Procházková, G., Šafařík, I., Brányik, T., 2012. Surface modification of Chlorella vulgaris cells using magnetite particles. Prcedia Eng. 42, 1778–1787. https://doi.org/10.1016/j.proeng.2012.07.572.

Rahman Bhuiyan, M.A., Mizanur Rahman, M., Shaid, A., Bashar, M.M., Khan, M.A., 2016. Scope of reusing and recycling the textile wastewater after treatment with gamma radiation. J. Clean. Prod. 112, 3063–3071. https://doi.org/10.1016/j.jclepro.2015.10.029.

Saavedra, R., Muñoz, R., Elisa, M., Vega, M., Bolado, S., 2018. Bioresource Technology Comparative uptake study of arsenic , boron , copper , manganese and zinc from water by di ff erent green microalgae. Bioresour. Technol. 263, 49–57. https://doi.org/10.1016/j.biortech.2018.04.101.

Schwertmann, U., Cornell, R.M., 2000. Iron Oxides in the Laboratory: Preparation and Characterization, 2nd Compl ed.

Srivastava, R.R., Kim, M.S., Lee, J.C., Ilyas, S., 2015. Liquid-liquid extraction of rhenium (VII) from an acidic chloride solution using Cyanex 923. Hydrometallurgy 157, 33–38. https://doi.org/10.1016/j.hydromet.2015.07.011.

Suresh Kumar, K., Dahms, H.U., Won, E.J., Lee, J.S., Shin, K.H., 2015. Microalgae - a promising tool for heavy metal remediation. Ecotoxicol. Environ. Saf. 113, 329–352. https://doi.org/10.1016/j.ecoenv.2014.12.019.

Taştan, B.E., Ertuğrul, S., Dönmez, G., 2010. Effective bioremoval of reactive dye and heavy metals by Aspergillus versicolor. Bioresour. Technol. 101, 870–876. https://doi.org/10.1016/j.biortech.2009.08.099.

United Nations A/RES/70/1, 2015. Transforming Our World: the 2030 Agenda for Sustainable Development, Governing through Goals: Sustainable Development Goals as Governance Innovation. https://doi.org/10.1057/978-1-137-45443-0_24.

United Nations Department for Economic and Social Affairs, 2013. World Economic and Social Survey 2013: Sustainable Development Challenges, Economic and Social Affairs.

United Nations World Water Development, 2003. Water for People, Water for Life. World Water Assesment Programme.

Varma, G., Misra, A.K., 2018. Indoor and Built Copper Contaminated Wastewater – an Evaluation of Bioremedial Options, vol. 27, pp. 84–95. https://doi.org/10.1177/1420326X16669397.

Vieira de Mendonça, H., Assemany, P., Abreu, M., Couto, E., Maciel, A.M., Duarte, R.L., Barbosa dos Santos, M.G., Reis, A., 2021. Microalgae in a global world: new solutions for old problems? Renew. Energy 165, 842–862. https://doi.org/10.1016/j.renene.2020.11.014.

Volesky, B., 2007. Biosorption and me. Water Res. 41, 4017–4029. https://doi.org/10.1016/j.watres.2007.05.062.

Wang, L., Zhang, C., Gao, F., Mailhot, G., Pan, G., 2017. Algae decorated TiO2/Ag hybrid nanofiber membrane with enhanced photocatalytic activity for Cr(VI) removal under visible light. Chem. Eng. J. 314, 622–630. https://doi.org/10.1016/j.cej.2016.12.020.

Zeraatkar, A.K., Ahmadzadeh, H., Talebi, A.F., Moheimani, N.R., McHenry, M.P., 2016. Potential use of algae for heavy metal bioremediation, a critical review. J. Environ. Manag. 181, 817–831. https://doi.org/10.1016/j.jenvman.2016.06.059.

Znad, H., Al Ketife, A.M.D., Judd, S., AlMomani, F., Vuthaluru, H.B., 2018. Bioremediation and nutrient removal from wastewater by Chlorella vulgaris. Ecol. Eng. 110, 1–7. https://doi.org/10.1016/J.ECOLENG.2017.10.008.